Research Square

Preprints are preliminary reports that have not undergone peer review.
They should not be considered conclusive, used to inform clinical practice,
or referenced by the media as validated information.

Magnitude of biome shifts over the last 21,000 years reveals the impact of seasonality and intense warming on future vegetation

Ulrike Herzschuh

Ulrike.Herzschuh@awi.de

Alfred Wegener Institute Helmholtz centre for Polar and Marine Research https://orcid.org/0000-0003-0999-1261

Chenzhi Li

Alfred Wegener Institute Helmholtz Centre for Polar and Marine Research https://orcid.org/0000-0002-9654-5245

Anne Dallmeyer

Max Planck Institute for Meteorology https://orcid.org/0000-0002-3270-610X

Article

Keywords:

Posted Date: June 16th, 2026

DOI: https://doi.org/10.21203/rs.3.rs-9993738/v1

License: This work is licensed under a Creative Commons Attribution 4.0 International License.
Read Full License

Additional Declarations: There is **NO** Competing Interest.

Magnitude of biome shifts over the last 21,000 years reveals the impact of seasonality and intense warming on future vegetation

Authors: Chenzhi Li[1,2], Anne Dallmeyer[3]*, Ulrike Herzschuh[1,2,4]*

Affiliations:

[1] Polar Terrestrial Environmental Systems, Alfred Wegener Institute Helmholtz Centre for Polar and Marine Research, Telegrafenberg A45, 14473 Potsdam, Germany

[2] Institute of Environmental Science and Geography, University of Potsdam, Karl-Liebknecht-Straße 24-25, 14476 Potsdam, Germany

[3] Max Planck Institute for Meteorology, Bundesstraße 53, 20146 Hamburg, Germany

[4] Institute of Biochemistry and Biology, University of Potsdam, Karl-Liebknecht-Straße 24-25, 14476 Potsdam, Germany

***Correspondence to:** Ulrike Herzschuh (Ulrike.Herzschuh@awi.de); Anne Dallmeyer (anne.dallmeyer@mpimet.mpg.de)

Abstract. Ongoing global warming and intensified human disturbance are projected to substantially alter future biome dynamics. However, robust prediction of such shifts requires long-term, spatially extensive datasets to evaluate model performance. Here, we integrate pollen-based biome reconstructions from a global compilation of 3,420 fossil records with simulations from the Max Planck Institute Earth System Model (MPI-ESM) to detect and attribute biome shifts over the past 21,000 years. Our results show that currently non-forested regions and ecotones have undergone more frequent biome shifts than forested and intra-biome areas since the Last Glacial Maximum (LGM). In the Northern Hemisphere, biome changes were particularly pronounced during the LGM–Lateglacial period, characterized by elevated compositional turnover and frequent biome-type transitions, driven by rapid growing season warming and enhanced seasonality. In contrast, anthropogenic-driven compositional turnover over the past 2,000 years surpassed that induced by LGM–Lateglacial climate change, but did not result in biome-type shifts. Future projections based on MPI-ESM simulations under a high-emission scenario (RCP 8.5) suggest that ecotones and non-forested regions—particularly those subject to increasing seasonality and warming—are likely to experience the most substantial biome shifts over the next 300 years.

1. Introduction

Ongoing global warming is altering the distribution and composition of plant biomes[1,2]. For example, warming-induced physiological stress and increased fire activity are driving boreal-to-temperate forest transitions at southern margins, such as in southern Scandinavia and the central Rocky Mountains[3,4]. In the Amazon, prolonged droughts and weakening ecosystem resilience are promoting the savannization of tropical forests[5,6]. However, directly attributing these observed shifts to recent climate forcing remains challenging, owing to the brevity of observational records, pervasive anthropogenic disturbances, and asynchronous responses across biomes[2,7]. These limitations underscore the need for long-term, spatially comprehensive assessments to robustly detect and attribute climate-driven biome shifts.

Pollen records and Earth System Models (ESMs) are useful tools for detecting and attributing biome shifts across long temporal spans and broad spatial scales[1,8]. However, most pollen-based studies to date have been, firstly, conducted at continental scales, where biome-level signals are aggregated, obscuring the heterogeneous responses of individual biomes; secondly, focused primarily on gradual changes in biome composition rather than on categorical transitions between biome types; and thirdly, limited to temporal scales while ignoring spatial patterns[9,10]. Furthermore, no ESM-based studies of biome shifts have been reported so far, as long-term and large-scale ESM-based biome simulations have rarely been performed[8,11].

Most studies on the climatic drivers of biome shifts to date have focused on annual trends and extremes, such as mean annual temperature or warmest-month temperature[1,7]. In contrast, seasonality—defined as intra-annual variability in monthly temperature or precipitation, typically measured as the standard deviation across 12 months[12]—has received comparatively little attention[13,14]. This neglect stems from two primary factors: limited availability of monthly-resolved climate data over long timescales, and a prevailing assumption that seasonality remains relatively constant through time[13,15]. However, reliance on seasonality is a defining feature of almost all natural biomes, and although it is intensifying under global warming, its ecological consequences have been vastly underappreciated[16,17].

Here, we examine the spatio-temporal dynamics of biome shifts using a recently synthesized global biome dataset developed by Li et al.[18]. This dataset integrates pollen-based biome reconstructions with output from a single transient simulation of the Max Planck Institute Earth System Model (MPI-ESM[8,19]), from which static biome distributions were derived at 500-year intervals over the past 21,000 years for 3,680 globally distributed sites. Building on this framework, we aim to (a) characterize the spatial and temporal patterns of biome shifts since the Last Glacial Maximum, (b) identify their climatic

drivers, and (c) project future biome trajectories and pinpoint regions most vulnerable to climate-driven transformation.

2. Results

Spatial patterns of global biome shifts since the Last Glacial Maximum

To assess long-term biome dynamics, we quantified the frequency of categorical biome shifts at global sites over the past 21,000 years using both pollen-derived reconstructions and ESM-based simulations (Fig. 1). A categorical biome shift is defined as a transition from one biome type to another between consecutive 500-year timeslices, and its frequency was calculated as the proportion of such shifts across all available timeslices at each site. Results indicate that sites located in currently non-forested regions—such as savanna (i.e., warm savanna and dry woodland), steppe (grassland and dry shrubland), desert (warm desert), and tundra (tundra and polar desert)—exhibit significantly higher shift frequencies than those in forested regions (i.e., tropical, subtropical, temperate, and boreal forests), in both the reconstruction and the simulation (Fig. 1c). In the reconstruction, the mean shift frequency for non-forested sites is 0.28, compared to 0.17 for forested sites (Wilcoxon test: $p < 0.05$). A similar but smaller difference is observed in the simulation (0.07 vs. 0.06; Wilcoxon test: $p < 0.05$).

In addition, sites located in currently ecotonal regions (i.e., transition zones between adjacent biomes) also exhibit significantly higher biome shift frequencies than those situated within the intra-biome regions, as evidenced in both the pollen-based reconstruction and the ESM-based simulation. Notable examples include ecotones in the East African Plateau, southern Andes, central Rocky Mountains, southern Scandinavia, and southern Alps, all of which display markedly elevated shift frequencies (Fig. 1). This spatial pattern is further supported by a distance-decay gradient: shift frequencies decline significantly with increasing distance from modern biome boundaries, with the highest values recorded at sites closest to those boundaries (Kruskal–Wallis test: $p < 0.001$; Fig. 1d).

Temporal patterns of biome dynamics in the Northern Hemisphere

To assess temporal patterns of biome compositional change, we used the Earth Mover's Distance (EMD[20]; see Methods) which quantifies turnover in the relative abundance of plant taxa between consecutive timeslices (Fig. 2a). The results reveal that compositional turnover in the Northern Hemisphere was significantly higher during the LGM-Lateglacial period (21–11.5 calibrated thousand years before present, where "present" refers to 1950 C.E.) than during the Holocene (<11.5 cal. ka BP), with median EMD values of 0.21 and 0.18, respectively (Wilcoxon test: $p < 0.05$). Notably, turnover

rose again in the past 2,000 years, peaking at 0.24 in low- and mid-latitude biomes such as subtropical forest, temperate forest, and savanna—indicating a renewed acceleration of vegetation change in the late Holocene.

The temporal pattern of the proportion of categorical biome shifts, calculated as the fraction of biome transitions among all available site pairs at timeslices, closely mirrors that of compositional turnover. This proportion was significantly higher during the LGM–Lateglacial period than during the Holocene, in both the pollen-based reconstruction (median 0.27 vs. 0.19; Wilcoxon test: $p < 0.05$; Fig. 2b) and the ESM-based simulation (median 0.10 vs. 0.03; Wilcoxon test: $p < 0.05$; Fig. 2c). Moreover, the temporal trajectories of biome shifts from both sources are positively correlated with compositional turnover, with Gaussian kernel correlation coefficients of $R = 0.68$ for the reconstruction and $R = 0.52$ for the simulation ($p < 0.01$; Supplementary Fig. 1). In contrast to compositional turnover, however, the proportion of biome shifts shows no clear increase over the past 2,000 years (Fig. 2b, c), neither in the simulation nor in the reconstructions.

Temporal correlations between bioclimate and biome dynamics in the Northern Hemisphere

Over the past 21,000 years in the Northern Hemisphere, both biome compositional turnover and categorical biome shifts exhibit stronger correlations with climate seasonality than with annual means or extremes (Fig. 3a; Supplementary Fig. 2a). Climate seasonality, defined as a composite index of temperature and precipitation seasonality (see Methods), shows a significant correlation with biome compositional turnover (Gaussian kernel correlation coefficient $R = 0.47$, $p < 0.05$). The corresponding correlations for the proportion of biome shifts are 0.68 for the pollen-based reconstruction and 0.53 for the ESM-based simulation (Supplementary Data 2).

Among all bioclimatic change rates, the rate of change in growing season temperature—calculated as a composite index reflecting relative changes in the temperature of the wettest and warmest quarters between consecutive timeslices—shows the strongest temporal correlation with biome dynamics. Specifically, Gaussian kernel correlation coefficients ($p < 0.01$) are $R = 0.52$ for compositional turnover, $R = 0.44$ for the proportion of biome shifts in the pollen-based reconstruction, and $R = 0.86$ in the ESM-based simulation (Fig. 3b; Supplementary Fig. 2b).

Future climate risk and biome shifts in the Northern Hemisphere

Building on our earlier finding that biome dynamics are most closely linked to climate seasonality and the rate of change in growing season temperature (Fig. 3), we assessed the spatial distribution of climate-driven biome change risk across the Northern Hemisphere under a high-emission scenario (RCP 8.5[21]). “High-risk regions” were defined as areas projected to experience both, elevated climate seasonality and rapid warming relative to pre-industrial conditions (i.e., timeslice 0.1 cal. ka BP),

indicating increased potential for climate-induced biome shifts over the next 300 years. According to MPI-ESM climate simulations, these regions are predominantly located in mid-latitude arid and semi-arid zones (e.g., the western United States, Mediterranean basin, and western and central Asia), high-latitude areas (e.g., eastern Siberia), and parts of the Sahel (Figs. 4a–4c).

We further quantified the magnitude of simulated biome shifts at 2250 C.E., relative to pre-industrial baselines, using a distance-based metric that incorporates both vegetation structure and bioclimatic zone preferences (see Methods). According to the MPI-ESM biome simulations, the greatest shift magnitudes are projected in currently non-forested regions, where the mean value reaches 1.50, compared to 0.83 in forested regions (Fig. 4d; Supplementary Table 1).

Overall, the spatial patterns of projected climate-driven biome risk levels and simulated biome shift magnitudes are broadly aligned across the Northern Hemisphere (Figs. 4a–4d). That is, regions projected to experience heightened climate seasonality and rapid warming over the next 300 years tend also to exhibit larger simulated biome shifts at 2250 C.E. (Fig. 4e). However, this spatial correspondence is not complete. Notably, 77.3% of grid cells identified as climatically high risk but showing no simulated biome shift are located in modern steppe and desert biomes, such as those in western Asia and the Sahara.

3. Discussion

Frequent biome shifts in currently non-forested regions and ecotones over the last 21,000 years

Globally, currently non-forested regions have experienced more frequent biome shifts than forested regions over the past 21,000 years, as consistently indicated by both our pollen-based reconstruction and ESM-based simulation of biome patterns (Fig. 1c). This disparity likely reflects the greater climatic variability and susceptibility to external disturbances—such as wildfires and insect outbreaks—that typify non-forested landscapes, in addition to their generally lower ecological resistance compared to forested systems. For example, semi-arid steppes are commonly subjected to more frequent fire regimes than forests[22,23], due to their drier and more variable bioclimatic conditions and the dominance of annual grasses over woody plant functional types (PFTs), which leads to the rapid accumulation of highly flammable biomass[24,25]. In contrast, forested regions typically support more diverse and productive PFT assemblages, enhancing their ecological resilience and conferring greater stability under equivalent climatic stress[26,27]. These results suggest that non-forested biomes have historically been more dynamic and may continue to be disproportionately vulnerable to biome shifts in the face of ongoing climate change.

Biome transition zones (i.e., ecotones) also show a higher frequency of biome shifts than intra-biome regions in both the reconstructions and simulations, challenging the long-held assumption of their inherent stability[27,28]. While geographic proximity to multiple biomes and climatic overlap have been hypothesized to enhance PFT diversity and buffer ecological responses via the so-called "edge effect"[27,29], our findings suggest a more complex reality. The taxonomically and functionally heterogeneous PFT assemblages characteristic of ecotones are more likely to reflect transitional or non-equilibrium states shaped by niche overlap and heightened competition, rendering these regions particularly sensitive to even subtle climatic perturbations or external forcing[30].

Climate-induced biome changes in the Northern Hemisphere over the last 21,000 years

Our results indicate that biome stability in the Northern Hemisphere over the past 21,000 years has been most strongly influenced by climatic seasonality, rather than by annual means or extremes[1,11] (Fig. 3a). In particular, during the LGM–Lateglacial period, elevated seasonality coincided with peaks in biome compositional turnover and categorical shifts (Fig. 2). High seasonality amplifies intra-annual variability in temperature and precipitation, disrupting resource availability and phenological timing[16,31]. Given that different plant PFTs possess distinct climatic tolerances and life-history traits, even modest seasonal fluctuations can substantially alter their relative performance and dominance. For example, in transitional zones such as the northern Amazon, increased precipitation seasonality may have reduced tropical tree cover while facilitating the expansion of raingreen shrubs and C4 grasses[32,33]. Similarly, in subtropical forests, seasonal cold extremes can impair evergreen tree function—through stomatal closure and reduced photosynthesis—giving cold-tolerant deciduous PFTs a competitive edge[34,35]. These effects are especially pronounced in non-forested biomes, where vegetation is strongly dependent on seasonal growth windows and particularly vulnerable to climatic perturbations[16,17]. For instance, elevated precipitation may trigger woody PFT encroachment in semi-arid steppe, while drought episodes can reduce herbaceous cover and destabilize community composition.

Additionally, we find that biome stability is particularly sensitive to the rate of change in growing season temperature, as evidenced by the highest temporal correlations observed in our analyses (Fig. 3b). Growing-season temperature plays a pivotal role in governing biome dynamics, as it regulates the establishment of PFTs constrained by thermal thresholds and shapes interspecific competition via differences in net primary productivity[36]. Temporal stability or variability in growing-season temperatures therefore directly influences both compositional turnover and biome shifts. In ecotonal regions such as the tundra–boreal forest boundary (e.g., northern Siberia), dominant woody taxa like *Betula*, *Alnus*, and *Salix* can adopt either shrub or tree forms depending on cumulative growing degree days. Consequently, fluctuations in growing-season warmth determine the competitive balance among boreal tree species, cold-resistant shrubs, and herbaceous taxa. This sensitivity is supported by

observational data showing northward expansion of boreal forests under ongoing climate warming and increasing growing degree days[4,37].

Anthropogenic-induced biome compositional turnover in the late-Holocene

In the Northern Hemisphere, biome compositional turnover increased markedly after 2 cal. ka BP, reaching the highest levels observed over the past 21,000 years (Fig. 2a). This pronounced rise is unlikely to have been driven by climatic factors, as the MPI-ESM simulation indicates relatively stable conditions during this period, characterized by low seasonality and minimal rates of change in growing-season temperature (Fig. 2d). Instead, the observed turnover is more plausibly attributed to intensified anthropogenic disturbances[9,38]—such as altered fire regimes, widespread deforestation, and the expansion of agriculture—as supported by archaeological records and land-use reconstructions[39,40]. Compared to earlier studies that identify the onset of significant human impact between 6 and 2.9 cal. ka BP[9,10], our results suggest a later regional signal. This difference likely stems from our inclusion of a more geographically diverse pollen dataset, particularly from areas beyond Europe and North America. Notably, no corresponding increase is evident in biome shifts at the categorical level during this period (Fig. 2b), indicating that late-Holocene anthropogenic pressures primarily altered vegetation composition rather than inducing large-scale biome type transitions.

Potential patterns of future biome shifts in the Northern Hemisphere

Under the high-emission and extreme warming scenario (RCP 8.5[21]), the MPI-ESM simulation projects widespread biome shifts across much of the Northern Hemisphere by 2250 C.E. (Fig. 4), with the most substantial changes expected in ecotones and non-forested regions, particularly across the circum-Arctic, mid-latitude arid and semi-arid zones, and the Sahel (Fig. 4d). These areas not only exhibited higher biome shift frequencies over the past 21,000 years (Figs. 1c, 1d), but also fall within zones of relatively high climatic risk, being projected to experience intensified seasonality and accelerated warming over the next 300 years relative to pre-industrial levels (Figs. 4a–4c). Nevertheless, the overall magnitude of simulated biome shifts remains moderate across these high-risk regions (Fig. 4e). Notably, 77.3% of grid cells identified as climatically high-risk yet lacking projected biome transitions are located in present-day steppe and desert regions, such as western Asia and the Sahara. This discrepancy may result from two key limitations: first, vegetation responses in arid and semi-arid environments are typically more sensitive to precipitation than temperature, rendering them less responsive in simulations driven primarily by thermal forcing[41]; and second, the MPI-ESM has historically underestimated biome dynamics in dryland regions (Fig. 1c), suggesting that its future projections may similarly underrepresent ecological sensitivity. Taken together, these findings emphasize the importance of

prioritizing ecotones and non-forested regions in biome conservation and climate adaptation strategies due to their heightened vulnerability under future climate change.

4. Methods

Pollen dataset and biome reconstruction

The fossil pollen data used in this study are sourced from the LegacyPollen 2.0 dataset, comprising 3,680 globally distributed palynological records[18,42]. A majority of these records (86.1%) originate from the Neotoma Paleoecology Database[43] (hereafter "Neotoma"), with additional contributions from the Abrupt Climate Change and Environmental Responses (ACER) 1.0 database[44], the Chinese fossil pollen dataset[45,46], and our own records[18]. To enhance comparability and ensure data quality, the compilation involved taxonomic harmonization (i.e., woody and major herbaceous taxa harmonized to the genus level, others to the family level[47]), temporal standardization (i.e., re-estimation of age–depth models[48]), and the inclusion of standardized metadata (e.g., data source, Neotoma ID, site name, coordinates, archive type, and references; see Supplementary Data 5). Further details on dataset synthesis are provided in Li et al.[42]. Although the dataset exhibits regional (most records located in the Northern Hemisphere) and temporal (declining record density with age) imbalances, it covers the world's major vegetation and climate zones (Supplementary Fig. 4).

We applied the biomization method of Prentice et al.[49]—a numerical approach that transforms pollen taxa and their relative abundances to biome categories via plant functional types (PFTs)—to reconstruct global biome distributions for 43 timeslices at 500-year intervals over the past 21,000 years[18]. Only records with consecutive timeslices (i.e., adjacent 500-year intervals) were included, resulting in a final dataset comprising 58,078 timeslices from 3,420 sites (Supplementary Data 6). Several methodological improvements were implemented relative to the standard biomization protocol[18]. First, the assignment of pollen taxa to PFTs was conducted separately for each continent, referencing existing regional biomization schemes and harmonized according to a globally standardized PFT classification[50,51]. Second, a coarser biome classification—termed "megabiomes" (hereafter "biomes")—was adopted to reflect large-scale vegetation patterns and match the categorical resolution of Earth System Model outputs, facilitating direct data–model comparisons[36]. These included tropical forest, subtropical forest, temperate forest, and boreal forest (collectively "forested biomes"), and warm savanna and dry woodland ("savanna"), grassland and dry shrubland ("steppe"), warm desert ("desert"), and tundra and polar desert ("tundra") (grouped as "non-forested biomes"). Third, to partially correct for pollen productivity biases, the abundances of *Larix* and *Pinus* were adjusted by multiplication factors of 15 and 0.5, respectively, prior to biome affinity calculations, following Bigelow et al.[52] and Cao et al.[11].

Finally, for each timeslice, the representative pollen sample was selected as the one closest in age within a ±250-year window—an interval optimized to balance chronological resolution and spatial coverage after evaluating narrower bin widths (e.g., 50 and 150 years).

Climate modeling and biome simulation

The transient simulation was performed with the Max-Planck-Institute Earth-System-Model version 1.2 (MPI-ESM[8,19]; spatial resolution ~3.75° × 3.75° on a Gaussian grid), which incorporates the land surface model JSBACH3[53] coupled with a dynamic vegetation module[54,55]. The experiment spans from 21 to 0 cal. ka BP, forced by prescribed orbital parameters[56], greenhouse gas concentrations[57], and continental ice-sheet reconstructions from GLAC-1D[58]. Bathymetry, topography, and river routing were updated at 10-year intervals. In addition, meltwater flux from the Laurentide Ice Sheet was modified for the interval between 15.2 and 11.8 cal. ka BP to simulate meltwater storage and release from proglacial lakes. The simulation was extended an additional 300 years into the future under a high-emission scenario (RCP 8.5[21]). However, as continental ice sheets are prescribed in the model, they do not dynamically respond to future temperature increases. Crucially, the transient framework enables a continuous and physically consistent coupling between climate and dynamic vegetation, allowing vegetation to evolve over time in response to gradually shifting boundary conditions[59,60].

Dynamic vegetation in MPI-ESM is represented by eight distinct PFTs that coexist within each grid-cell[8]. The model distinguishes between extratropical and tropical trees—each classified as either evergreen or deciduous—along with raingreen and cold-tolerant shrubs, and both C3 and C4 grasses. The presence and distribution of PFTs are regulated by bioclimatic thresholds that reflect physiological requirements such as cold tolerance, chilling needs, and heat adaptation. Disturbances such as fire, already incorporated into the dynamic vegetation modules, periodically reduce the coverage of woody PFTs and favor the expansion of herbaceous types, whereas land use is not included in the module[8,53]. Shifts in PFT cover in response to climate variability are primarily driven by differences in annual net primary productivity, which determines competitive outcomes under conditions suitable for multiple PFTs. The establishment or decline of PFTs may occur within a few decades, depending on climatic conditions and inter-PFT competition, although tree PFTs generally respond more slowly than grasses and shrubs[54].

The simulated PFT fractions are translated into the same eight biome categories used in the pollen-based reconstructions using the classification tool described by Dallmeyer et al.[36]. This method assigns biome types based on predefined thresholds of PFT dominance combined with bioclimatic constraints that capture the climatic tolerances of various biome types. These constraints are primarily derived from the distribution of 2-meter air temperatures and align with the principles used in classical biome models

such as BIOME4[61], thereby ensuring conceptual consistency and comparability with the pollen-based biome reconstructions.

The simulation output was processed as 100-year climatological means. Specifically, the first timeslice at 21 cal. ka BP represents an average over the years 20,999–20,900 BP, while the final timeslice at 2,250 C.E. averages the period from 2,151 to 2,250 C.E. For each site, we extracted simulated climate and biome data from the corresponding grid cell and included only those site–timeslice combinations for which pollen-based reconstructions were available (see Supplementary Data 6).

Evaluation and shortcomings

The transient modeling experiments, pollen-based reconstructions, and ESM-based biome simulations were evaluated and demonstrated generally good performance. Specifically, the simulated climate trajectories effectively capture major climatic trends and states that align with multi-proxy reconstructions, established transient simulations, and modern instrumental datasets[8]. Similarly, biome distributions derived from both pollen-based reconstructions and ESM-based simulations broadly match modern potential natural biome patterns[36,62] (Supplementary Data 7), aggregated from potential natural vegetation datasets[63,62]. Site-level comparisons at 0 cal. ka BP ($n = 2{,}237$) indicate an overall agreement of 80.15% for the reconstructions and 65.67% for the simulations relative to modern potential biomes (Supplementary Table 3). Nonetheless, certain biome types, particularly steppe and tundra, exhibit lower accuracy (~50% agreement), consistent with results from earlier biomization efforts[52,64]. For example, in the northern margin of the East Asian summer monsoon region, high pollen productivity of *Artemisia* may lead to steppe overrepresentation[65]. On the Tibetan Plateau, distinguishing tundra from steppe is hindered by low taxonomic resolution and the dominance of shared taxa such as Poaceae and Cyperaceae (Supplementary Figs. 5a, 5c). The model simulations also show systematic spatial biases (Supplementary Figs. 5b, 5d). In high-elevation regions such as the central-southern Rocky Mountains and central Andes, limited agreement may stem from excessive surface warming associated with smoothed topography at the model's coarse spatial resolution (~3.75° × 3.75°). In the Mediterranean region, the ESM simulates non-forest biomes where forests are expected, likely due to biases in simulated seasonal climate—specifically, overly hot summers and dry winters[18,8].

A comparison between the MPI-ESM simulation and a similar pollen-based biome reconstruction revealed a temporal mismatch of approximately 4,000 years in the timing of deglacial forest expansion across the Northern Hemisphere[8]. This discrepancy is also evident in our reconstruction, albeit to a lesser extent. The underlying causes of this mismatch remain uncertain. It is possible that methodological limitations, including missing processes in the model, contribute to the deviation. Moreover, differences in biome definitions—based on temperature thresholds in the model versus actual plant composition in the reconstruction—may lead to discrepancies in biome classification,

particularly within transition zones. Additionally, the model simulates only natural vegetation in quasi-equilibrium with climate and does not account for anthropogenic land use. Despite these limitations, we consider both the simulation and the reconstruction to be robust, given the overall consistency in long-term trends and close agreement with modern biome distributions.

Compositional turnover and categorical shift in biomes

To quantify biome compositional turnover, we calculated the Earth Mover's Distance (EMD[20]) between consecutive timeslices based on pollen-type percentage data at each site. EMD quantifies dissimilarity as the minimum "work" required to transform one taxonomic distribution into another, with higher values indicating greater compositional change. By incorporating the full distribution of pollen-type abundances, this approach captures subtle or gradual shifts in vegetation composition beyond changes in dominant taxa. Calculations and statistical testing were performed using the *EMD()* and *signif_threshold()* functions from the *paleotools* package (version 0.1.0[66]) in R (version 4.4.1[67]). For each timeslice pair, 100 synthetic assemblages were generated for each sample by adding random noise (±0.01) to the relative abundances of individual taxa, followed by renormalization. These 200 synthetic assemblages were combined, and 500 random EMD comparisons were computed between them to generate a null distribution. The 95th percentile of this null distribution was used as the significance threshold. Observed EMD values exceeding this threshold were classified as statistically significant compositional changes (Supplementary Data 1).

We defined a biome shift as a categorical change in the assigned biome between two consecutive 500-year timeslices at a given site, in both the pollen-based reconstruction and the ESM-based simulation. For each site, we calculated the proportion of these categorical shifts relative to the total number of available consecutive timeslice pairs spanning the past 21,000 years (Supplementary Data 1).

To investigate temporal patterns in biome dynamics, we grouped pollen records from the Northern Hemisphere into eight biome clusters, based on their spatial distribution within modern potential natural biome regions. For each timeslice within each cluster, we computed the median of only those EMD values that exceeded their respective significance thresholds, thereby capturing ecologically meaningful compositional turnover. The frequency of biome shifts was calculated as the proportion of categorical biome transitions among all available site pairs. To derive hemispheric-scale metrics, cluster-level values were aggregated using area-weighted means, with weights reflecting the proportional extent of each biome cluster within the modern potential natural vegetation distribution (Supplementary Table 4).

Bioclimatic variables

To characterize long-term climatic conditions at each site, we derived 14 bioclimatic variables from monthly temperature and precipitation data simulated by MPI-ESM over the past 21,000 years. These variables include: annual mean temperature; temperature seasonality (calculated as the standard

deviation of monthly temperatures × 100); mean temperature of the wettest, driest, warmest, and coldest quarters; annual precipitation; precipitation of the wettest and driest months; precipitation seasonality (expressed as the coefficient of variation); and precipitation totals for the wettest, driest, warmest, and coldest quarters (following O'Donnell and Ignizio[12]). Temperature values are reported in degrees Celsius (°C) and precipitation in millimetres (mm). Together, these variables capture patterns of annual climate means, seasonality, and extremes or limiting climatic conditions. To assess temporal variability, we also calculated the rate of change in each variable between consecutive timeslices, defined as the magnitude of relative change (see Supplementary Data 3 and 8).

As with the biome metrics, we extracted time series of simulated bioclimatic variables and their corresponding rates of change for each modern potential natural biome region in the Northern Hemisphere. To enable direct comparisons and minimize dimensional inconsistencies among variables, all time series were normalized to a 0–1 scale.

We conducted hierarchical clustering on the time series of 14 hemispheric bioclimatic variables using the *tsclust()* function from the R package *dtwclust* (version 6.0.0[68]). To reduce dimensionality and highlight dominant climatic gradients, these variables were aggregated into five composite bioclimatic indices: (1) bioclimate seasonality = temperature seasonality + precipitation seasonality; (2) non-growing season temperature ($T_{non\text{-}growing}$) = annual mean temperature + mean temperature of the driest quarter + mean temperature of the coldest quarter; (3) growing season temperature ($T_{growing}$) = mean temperature of the wettest quarter + mean temperature of the warmest quarter; (4) growing season precipitation ($P_{growing}$) = annual precipitation + precipitation of the wettest month + precipitation of the wettest quarter + precipitation of the warmest quarter; and (5) non-growing season precipitation ($P_{non\text{-}growing}$) = precipitation of the driest month + precipitation of the driest quarter + precipitation of the coldest quarter (Supplementary Fig. 3). For each timeslice, both the composite value and its rate of change were calculated as the median of the normalized component variables.

Potential spatial patterns of future bioclimates and biome shifts

To assess future changes in climate and vegetation, we quantified both the absolute values and rates of change of five composite bioclimatic variables across MPI-ESM grid-cells (spatial resolution: ~3.75° × 3.75°) in the Northern Hemisphere for the next 300 years. Specifically, we first calculated the five composite variables from the 14 normalized bioclimatic variables at all grid-cells with known modern biome distributions for three future timeslices (i.e., 2050, 2150, and 2250 C.E., each representing a 100-year climatological mean). In parallel, we computed the rates of change for each variable relative to pre-industrial conditions (i.e., the 0.1 cal. ka BP timeslice). For each variable, both the state and rate of change were binned into quantile intervals (25th, 50th, 75th, and 100th percentiles). By combining quantile classes of two composite variables or their respective change rates, we

constructed a 4 × 4 contingency matrix comprising 16 bioclimatic categories (Fig. 4), which allowed us to identify bioclimatic conditions associated with an elevated likelihood of biome shifts.

To quantify the magnitude of biome shifts between the future timeslice (2,250 C.E.) and pre-industrial conditions, we constructed a distance matrix based on differences in vegetation structure and bioclimatic zone preferences. Vegetation structure was classified into three categories: forest, non-forest, and desert. Bioclimatic zones were categorized as tropical, subtropical, temperate, boreal, and polar[69,70]. In the distance matrix, two biomes that share either the same vegetation structure or bioclimatic zone were assigned a baseline distance of one. Each additional mismatch in structure or climate zone added one unit to the distance score (Supplementary Table 5). For instance, temperate forest differs by one unit from boreal forest, but by three units from desert.

We subsequently quantified both the frequency and magnitude of biome shifts between the pre-industrial baseline and the future timeslice (2,250 C.E.) across the Northern Hemisphere, stratified by the bioclimatic matrix classes described above. For each combination of composite bioclimatic variables, biome shift frequency was defined as the proportion of grid-cells within a given class that experienced a biome shift. Biome shift magnitude was calculated as the mean ecological–bioclimatic distance of all shifting grid-cells within that class.

Statistical analyses

We applied Gaussian kernel correlation to quantify temporal similarity between time series, using the *nest* package (version 1.05.44[71]) in R. This correlation-based estimator is particularly well-suited for comparing time series with irregular temporal resolution and differing measurement units[72,73].

To assess differences between groups—such as the proportion of biome shifts between reconstruction- and simulation-based datasets—we used non-parametric, rank-based statistical tests. For pairwise comparisons, we employed the Wilcoxon rank-sum test (via the *wilcox.test()* function in R), and for comparisons involving three or more independent groups, we used the Kruskal–Wallis rank-sum test (via *kruskal.test()* in R). Both tests evaluate whether group medians differ significantly and are robust to violations of normality and heteroscedasticity[74].

Data availability

The LegacyPollen 2.0 dataset used in this study is publicly available through PANGAEA at https://doi.org/10.1594/PANGAEA.965907[42] (last access: 26 September 2024). The taxa-to-PFT and PFT-to-biome assignment lists employed in the biomization procedure can be accessed via the GWDG

Cloud at https://owncloud.gwdg.de/index.php/s/M0d8cuJpkxqhOH4 (last access: 16 May 2024). The input data from the MPI-ESM simulation used for biomization are available from the World Data Center for Climate (WDCC) at https://doi.org/10.26050/WDCC/PMMXMCHTD[75] (last access: 16 May 2024). The modern potential natural vegetation dataset by Ramankutty et al.[62] is available at https://daac.ornl.gov/cgi-bin/dsviewer.pl?ds_id=961 (last access: 16 May 2024). All source data supporting the statistical analyses and figures are provided in Supplementary Data 1–8.

Code availability

All statistical analyses and visualizations presented in this study were conducted using the R software. The corresponding R scripts have been archived in a public GitHub repository and are accessible at: https://github.com/PolarTerrestrialEnvironmentalSystems/Biome-shift (last accessed: 21 June 2025). The tool used for the biomization of simulated PFT cover fractions is available from the MPG.PuRe repository at https://hdl.handle.net/21.11116/0000-0001-B800-F[36] (last accessed: May 16, 2024).

Acknowledgements

The majority of fossil pollen data used in this study were obtained from the Neotoma Paleoecology Database (https://www.neotomadb.org/; last access: 31 August 2022) and its constituent repositories (e.g., APD, EPD, ALPADABA, IPPD, LAPD, and NAPD). We gratefully acknowledge the efforts of all data contributors, data stewards, and the broader Neotoma community. We thank all palynologists and geologists who directly or indirectly contributed pollen data and chronologies to the database. We also thank John W. Williams and Thomas Giesecke (Neotoma Paleoecology Database) for their valuable comments on the compilation of the LegacyPollen 2.0 dataset (https://doi.org/10.5194/essd-2023-486-CC3; https://doi.org/10.5194/essd-2023-486-RC2). Thomas Böhmer is acknowledged for his assistance in revising the R scripts. We thank Thomas Kleinen (Max Planck Institute for Meteorology) for providing the MPI-ESM simulation and Cathy Jenks for language editing on an earlier version of the manuscript.

This research was supported by the European Research Council (ERC Glacial Legacy, grant no. 772852 to U.H.) and the PalMod Initiative (grant no. 01LP1510C to U.H.). A.D. is funded by the German Federal Ministry of Education and Research (BMBF) as part of the Research for Sustainability (FONA) initiative, through the PalMod Phase II and III projects (grant nos. 01LP1920A and 01LP2306A). C.L. is supported by a scholarship from the China Scholarship Council (grant no. 201908130165).

Author contributions

U.H. and C.L. conceived and designed the study. C.L. conducted the pollen-based biome reconstruction, and A.D. performed the model-based biomization. C.L. carried out the data analysis and wrote the initial draft of the manuscript under the supervision of U.H. and A.D. All authors contributed to the interpretation of results and to the final version of the manuscript.

Competing interests

All authors declare no competing interests.

References

1. Nolan, C. *et al.* Past and future global transformation of terrestrial ecosystems under climate change. *Science* **361**, 920–923 (2018).
2. Higgins, S. I., Conradi, T. & Muhoko, E. Shifts in vegetation activity of terrestrial ecosystems attributable to climate trends. *Nat. Geosci.* **16**, 147–153 (2023).
3. Rao, M. P. *et al.* Approaching a thermal tipping point in the Eurasian boreal forest at its southern margin. *Commun. Earth Environ.* **4**, 1–10 (2023).
4. Xi, Y., Zhang, W., Wei, F., Fang, Z. & Fensholt, R. Boreal tree species diversity increases with global warming but is reversed by extremes. *Nat. Plants* **10**, 1473–1483 (2024).
5. Salazar, L. F. & Nobre, C. A. Climate change and thresholds of biome shifts in Amazonia. *Geophys. Res. Lett.* **37**, (2010).
6. Boulton, C. A., Lenton, T. M. & Boers, N. Pronounced loss of Amazon rainforest resilience since the early 2000s. *Nat. Clim. Change* **12**, 271–278 (2022).
7. Pecl, G. T. *et al.* Biodiversity redistribution under climate change: Impacts on ecosystems and human well-being. *Science* **355**, eaai9214 (2017).
8. Dallmeyer, A. *et al.* The deglacial forest conundrum. *Nat. Commun.* **13**, 6035 (2022).
9. Mottl, O. *et al.* Global acceleration in rates of vegetation change over the past 18,000 years. *Science* **372**, 860–864 (2021).
10. Gordon, J. D., Fagan, B., Milner, N. & Thomas, C. D. Floristic diversity and its relationships with human land use varied regionally during the Holocene. *Nat. Ecol. Evol.* **8**, 1459–1471 (2024).
11. Cao, X., Tian, F., Dallmeyer, A. & Herzschuh, U. Northern Hemisphere biome changes (>30°N) since 40 cal ka BP and their driving factors inferred from model-data comparisons. *Quat. Sci. Rev.* **220**, 291–309 (2019).
12. O'Donnell, M. S. & Ignizio, D. A. Bioclimatic predictors for supporting ecological applications in the conterminous United States. *U.S. Geological Survey Data Series* **691**, 1–10 (2012).
13. White, E. R. & Hastings, A. Seasonality in ecology: Progress and prospects in theory. *Ecol. Complex.* **44**, 100867 (2020).
14. Tonkin, J. D., Bogan, M. T., Bonada, N., Rios-Touma, B. & Lytle, D. A. Seasonality and predictability shape temporal species diversity. *Ecology* **98**, 1201–1216 (2017).
15. Fleitmann, D., Burns, S. J., Matter, A., Cheng, H. & Affolter, S. Moisture and seasonality shifts recorded in Holocene and Pleistocene speleothems from southeastern Arabia. *Geophys. Res. Lett.* **49**, e2021GL097255 (2022).
16. Feng, X., Porporato, A. & Rodriguez-Iturbe, I. Changes in rainfall seasonality in the tropics. *Nat. Clim. Change* **3**, 811–815 (2013).
17. Hajek, O. L. & Knapp, A. K. Shifting seasonal patterns of water availability: ecosystem responses to an unappreciated dimension of climate change. *New Phytol.* **233**, 119–125 (2022).

18. Li, C. *et al.* Global biome changes over the last 21 000 years inferred from model–data comparisons. *Climate of the Past* **21**, 1001–1024 (2025).
19. Mauritsen, T. *et al.* Developments in the MPI-M Earth System Model version 1.2 (MPI-ESM1.2) and Its Response to Increasing CO_2. *J. Adv. Model. Earth Syst.* **11**, 998–1038 (2019).
20. Chevalier, M. *et al.* Refining data–data and data–model vegetation comparisons using the Earth mover's distance (EMD). *Clim. Past* **19**, 1043–1060 (2023).
21. Riahi, K. *et al.* RCP 8.5—A scenario of comparatively high greenhouse gas emissions. *Clim. Change* **109**, 33 (2011).
22. Mouillot, F. & Field, C. B. Fire history and the global carbon budget: a 1°× 1° fire history reconstruction for the 20th century. *Global Change Biol.* **11**, 398–420 (2005).
23. Leys, B. A., Commerford, J. L. & McLauchlan, K. K. Reconstructing grassland fire history using sedimentary charcoal: Considering count, size and shape. *PLOS ONE* **12**, e0176445 (2017).
24. Poppenwimer, T., Mayrose, I. & DeMalach, N. Revising the global biogeography of annual and perennial plants. *Nature* **624**, 109–114 (2023).
25. Simpson, K. J. *et al.* Determinants of flammability in savanna grass species. *J. Ecol.* **104**, 138–148 (2016).
26. Southworth, J. *et al.* Latitudes and land use: Global biome shifts in vegetation persistence across three decades. *Front. Remote Sens.* **4**, (2023).
27. Schindler, D. E. *et al.* Population diversity and the portfolio effect in an exploited species. *Nature* **465**, 609–612 (2010).
28. Delcourt, P. A. & Delcourt, H. R. Ecotone dynamics in space and time. in *Landscape boundaries: consequences for biotic diversity and ecological flows* (eds. Hansen, A. J. & di Castri, F.) 19–54 (Springer, New York, NY). https://doi.org/10.1007/978-1-4612-2804-2_2 (1992).
29. Li, Z. *et al.* Stable or unstable? Landscape diversity and ecosystem stability across scales in the forest–grassland ecotone in northern China. *Landscape Ecol.* **38**, 3889–3902 (2023).
30. Neilson, R. P. Transient ecotone response to climatic change: some conceptual and modelling approaches. *Ecol. Appl.* **3**, 385–395 (1993).
31. Intergovernmental Panel on Climate Change (IPCC). Climate Change 2021 – The Physical Science Basis: Working Group I Contribution to the Sixth Assessment Report of the Intergovernmental Panel on Climate Change. (*Cambridge Univ. Press, 2023*). https://doi.org/10.1017/9781009157896.
32. Malhi, Y. *et al.* Responses of Amazonian ecosystems to climatic and atmospheric carbon dioxide changes since the last glacial maximum. *Philos. Trans. R. Soc. B Biol. Sci.* **359**, 499–514 (2004).
33. Hoffmann, W. A. Seasonal flooding shapes forest–savanna transitions. *Proc. Natl. Acad. Sci. U.S.A.* **120**, e2312279120 (2023).
34. McDowell, N. *et al.* Mechanisms of plant survival and mortality during drought: why do some plants survive while others succumb to drought? *New Phytol.* **178**, 719–739 (2008).

35. Zheng, Z. *et al.* Holocene warming and evergreen/deciduous forest replacement across eastern China. *Quat. Sci. Rev.* **307**, 108057 (2023).
36. Dallmeyer, A., Claussen, M. & Brovkin, V. Harmonising plant functional type distributions for evaluating Earth system models. *Clim. Past* **15**, 335–366 (2019).
37. Frost, G. V. & Epstein, H. E. Tall shrub and tree expansion in Siberian tundra ecotones since the 1960s. *Global Change Biol.* **20**, 1264–1277 (2014).
38. Marquer, L. *et al.* Quantifying the effects of land use and climate on Holocene vegetation in Europe. *Quat. Sci. Rev.* **171**, 20–37 (2017).
39. Stephens, L. *et al.* Archaeological assessment reveals Earth's early transformation through land use. *Science* **365**, 897–902 (2019).
40. Cao, X. Stability of Holocene pollen assemblages in eastern China disturbed by human activities over the last two millennia. *Sci. Bull.* https://doi.org/10.1016/j.scib.2025.03.031 (2025).
41. Weltzin, J. F. *et al.* Assessing the response of terrestrial ecosystems to potential changes in precipitation. *BioScience* **53**, 941–952 (2003).
42. Li, C. *et al.* LegacyPollen2.0: an updated global taxonomically and temporally standardized fossil pollen dataset of 3680 palynological records [dataset bundled publication]. PANGAEA. https://doi.org/10.1594/PANGAEA.965907 (2025).
43. Williams, J. W. *et al.* The Neotoma Paleoecology Database, a multiproxy, international, community-curated data resource. *Quat. Res.* **89**, 156–177 (2018).
44. Sánchez Goñi, M. F. *et al.* The ACER pollen and charcoal database: a global resource to document vegetation and fire response to abrupt climate changes during the last glacial period. *Earth Syst. Sci. Data* **9**, 679–695 (2017).
45. Zhou, B. *et al.* A fossil pollen dataset of China. Chin. J. Plant Ecol. 47, 1453–1463 (2023). https://doi.org/10.17521/cjpe.2022.0316. [In Chinese].
46. Cao, X. *et al.* Human activities have reduced plant diversity in eastern China over the last two millennia. *Global Change Biol.* **28**, 4962–4976 (2022).
47. Herzschuh, U. *et al.* LegacyPollen 1.0: a taxonomically harmonized global late Quaternary pollen dataset of 2831 records with standardized chronologies. *Earth Syst. Sci. Data* **14**, 3213–3227 (2022).
48. Li, C. *et al.* Harmonized chronologies of a global late Quaternary pollen dataset (LegacyAge 1.0). *Earth Syst. Sci. Data* **14**, 1331–1343 (2022).
49. Prentice, C., Guiot, J., Huntley, B., Jolly, D. & Cheddadi, R. Reconstructing biomes from palaeoecological data: a general method and its application to European pollen data at 0 and 6 ka. *Clim. Dyn.* **12**, 185–194 (1996).
50. Harrison, S. P. *et al.* Ecophysiological and bioclimatic foundations for a global plant functional classification. *J. Veg. Sci.* **21**, 300–317 (2010).
51. Harrison, S. BIOME 6000 DB classified plotfile version 1. University of Reading. https://doi.org/10.17864/1947.99 (2017).

52. Bigelow, N. H. *et al.* Climate change and Arctic ecosystems: 1. Vegetation changes north of 55°N between the last glacial maximum, mid-Holocene, and present. *J. Geophys. Res. Atmos.* **108**, (2003).
53. Reick, C. H. et al. JSBACH 3 - The land component of the MPI Earth System Model: documentation of version 3.2. Hamburg: MPI für Meteorologie. *Berichte zur Erdsystemforsch*, **240**. https://hdl.handle.net/21.11116/0000-0008-098B-2 (2021).
54. Reick, C. H., Raddatz, T., Brovkin, V. & Gayler, V. Representation of natural and anthropogenic land cover change in MPI-ESM. *J. Adv. Model. Earth Syst.* **5**, 459–482 (2013).
55. Brovkin, V., Raddatz, T., Reick, C. H., Claussen, M. & Gayler, V. Global biogeophysical interactions between forest and climate. *Geophys. Res. Lett.* 36, L07405 (2009).
56. Berger, A. Long-term variations of daily insolation and Quaternary climatic changes. *J. Atmos. Sci.* **35**, 2362–2367 (1978).
57. Köhler, P., Nehrbass-Ahles, C., Schmitt, J., Stocker, T. F. & Fischer, H. A 156 kyr smoothed history of the atmospheric greenhouse gases CO_2, CH_4, and N_2O and their radiative forcing. *Earth Syst. Sci. Data* **9**, 363–387 (2017).
58. Tarasov, L., Dyke, A. S., Neal, R. M. & Peltier, W. R. A data-calibrated distribution of deglacial chronologies for the North American ice complex from glaciological modeling. *Earth Planet. Sci. Lett.* **315–316**, 30–40 (2012).
59. Foley, J. A., Levis, S., Costa, M. H., Cramer, W. & Pollard, D. Incorporating dynamic vegetation cover within global climate models. *Ecol. Appl.* **10**, 1620–1632 (2000).
60. Dallmeyer, A., Claussen, M., Lorenz, S. J. & Shanahan, T. The end of the African humid period as seen by a transient comprehensive Earth system model simulation of the last 8000 years. *Clim. Past* **16**, 117–140 (2020).
61. Kaplan, J. O. *et al.* Climate change and Arctic ecosystems: 2. Modeling, paleodata-model comparisons, and future projections. *J. Geophys. Res. Atmos.* **108**, 8171 (2003). https://doi.org/10.1029/2002JD002559.
62. Ramankutty, N. *et al.* ISLSCP II Potential Natural Vegetation Cover. ORNL DAAC, Oak Ridge, Tennessee, USA. https://doi.org/10.3334/ORNLDAAC/961 (2010).
63. Ramankutty, N. & Foley, J. A. Estimating historical changes in global land cover: Croplands from 1700 to 1992. *Global Biogeochem. Cycles* **13**, 997–1027 (1999).
64. Marinova, E. *et al.* Pollen-derived biomes in the Eastern Mediterranean–Black Sea–Caspian-Corridor. *J. Biogeogr.* **45**, 484–499 (2018).
65. Xu, Q. et al. Relative pollen productivities of typical steppe species in northern China and their potential in past vegetation reconstruction. Sci. China Earth Sci. 57, 1254–1266 (2014).
67. R Core Team. R: A language and environment for statistical computing. R Foundation for Statistical Computing, Vienna, Austria. https://www.r-project.org/ (2023).
68. Sarda-Espinosa, A. dtwclust: Time Series Clustering Along with Optimizations for the Dynamic Time Warping Distance. https://github.com/asardaes/dtwclust (2024).

69. Allen, J. R. M. *et al.* Global vegetation patterns of the past 140,000 years. *J. Biogeogr.* **47**, 2073–2090 (2020).
70. Sato, H. *et al.* Dry corridors opened by fire and low CO_2 in Amazonian rainforest during the Last Glacial Maximum. *Nat. Geosci.* **14**, 578–585 (2021).
71. Rehfeld, K. nest: Nonlinear Earth System Trajectories – R package source code. https://rdrr.io/github/krehfeld/nest/src/R/nest-package.R (2019).
72. Rehfeld, K., Marwan, N., Heitzig, J. & Kurths, J. Comparison of correlation analysis techniques for irregularly sampled time series. *Nonlinear Process. Geophys.* **18**, 389–404 (2011).
73. Rehfeld, K. & Kurths, J. Similarity estimators for irregular and age-uncertain time series. *Clim. Past* **10**, 107–122 (2014).
74. Field, A., Field, Z. & Miles, J. Discovering Statistics Using R. London: Sage Publications (2012).
75. Kleinen, T., Gromov, S., Steil, B. & Brovkin, V. PalMod2 MPI-M MPI-ESM1-2-CR-CH4 future-methane. World Data Center for Climate (WDCC) at DKRZ https://doi.org/10.26050/WDCC/PMMXMCHfm (2023).

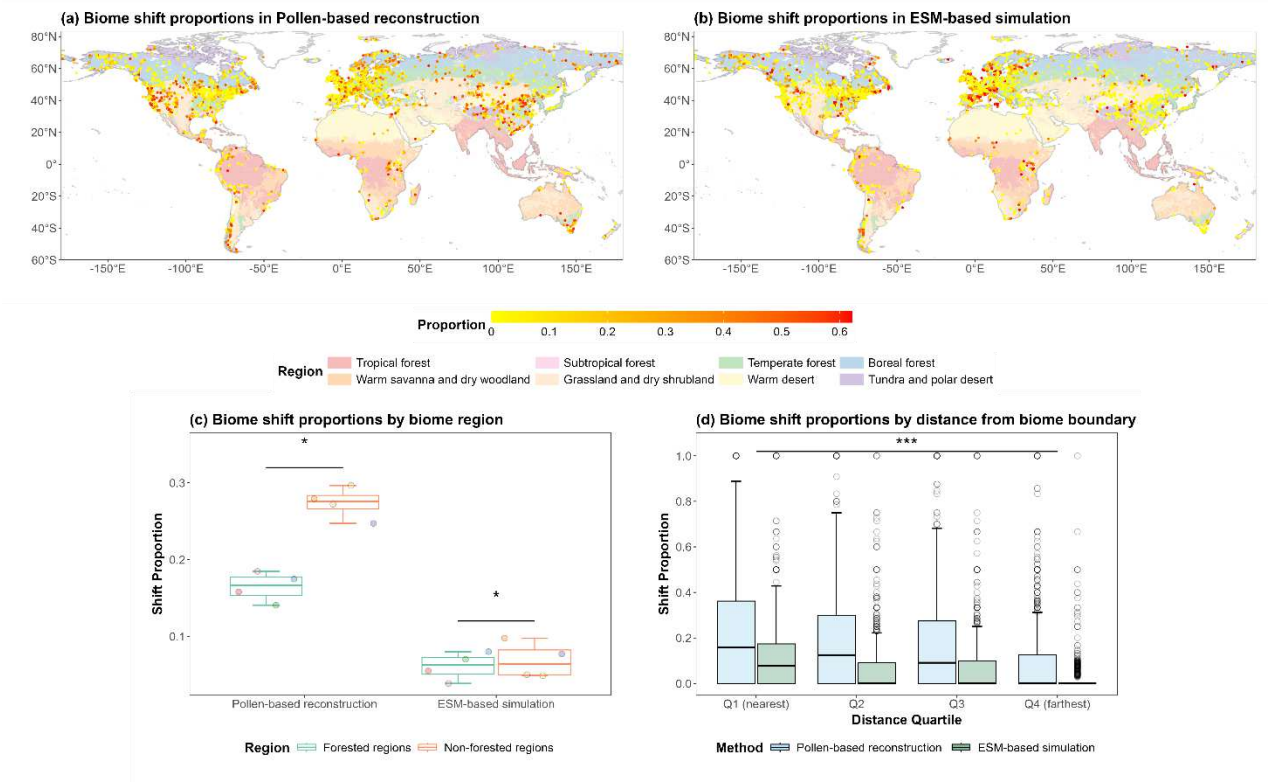


Fig. 1: Proportions of biome shifts over the last 21,000 years derived from a pollen-based reconstruction and an Earth system model (ESM)-based simulation. (a, b) Spatial distribution of site-level biome shift proportions in the pollen-based reconstruction and ESM-based simulation, respectively. To ensure visual comparability, ESM shift proportions are scaled (×2) to match the reconstruction range, and values exceeding the 95th percentile in both datasets are capped. The map background depicts the distribution of modern potential natural biomes aggregated from modern potential natural vegetation (5 arc-minute resolution[62,36]). **(c)** Biome shift proportions in forested and non-forested regions. Boxes represent interquartile ranges (IQR), whiskers 1.5 × IQR. Colored dots indicate biome-level means, with point colors matching those in panels (a) and (b). Asterisks denote significant differences in shift proportions between forested and non-forested regions ($p < 0.05$). Forested regions include tropical forest, subtropical forest, temperate forest, and boreal forest; non-forested regions include warm savanna and dry woodland, grassland and dry shrubland, warm desert, and tundra and polar desert. **(d)** Shift proportions by quartile of distance to biome boundary (Q1 = nearest, Q4 = farthest). Asterisks indicate a significant difference across quartiles ($p < 0.001$).

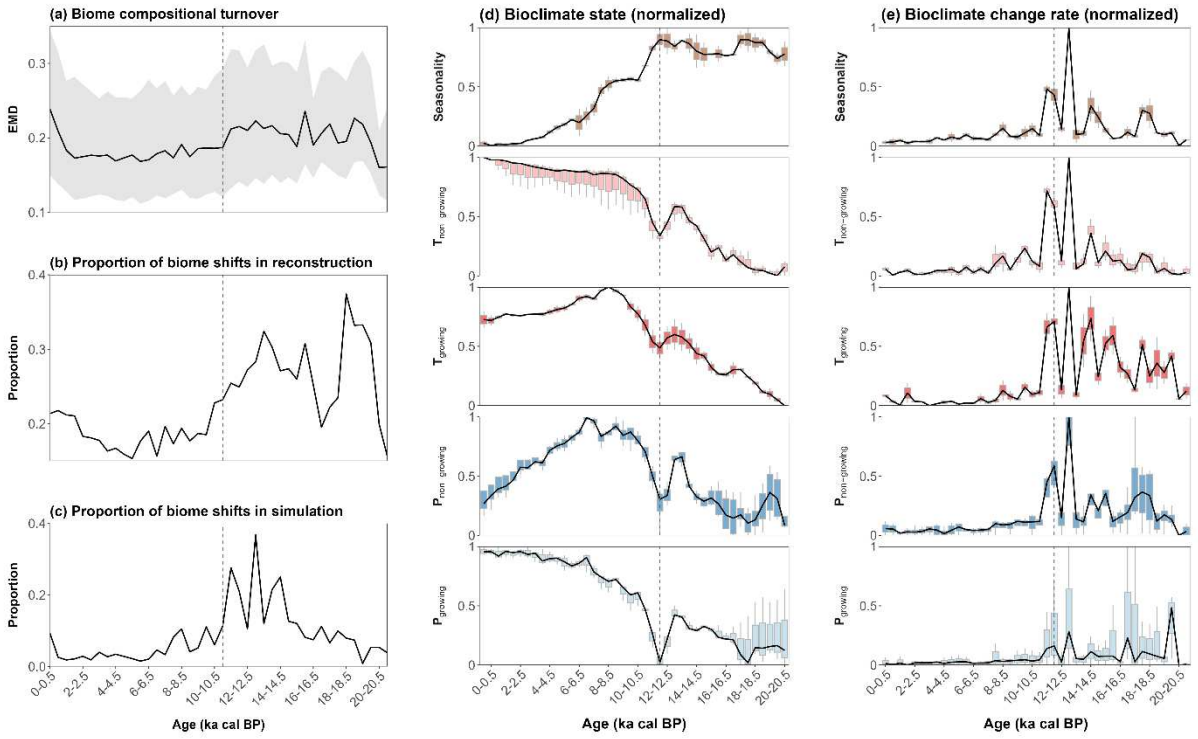


Fig. 2: Temporal dynamics of biome and bioclimatic change in the Northern Hemisphere over the past 21,000 years. (a) Median biome compositional turnover, expressed as Earth Mover's Distance (EMD[20]), with shaded areas indicating the interquartile range (25th–75th percentiles). (**b, c**) Proportions of categorical biome shifts derived from the pollen-based reconstruction (b) and ESM-based simulation (c). (**d, e**) Temporal trends in the state (d) and rate of change (e) of composite bioclimatic variables simulated by MPI-ESM[8,19], including seasonality, growing season temperature ($T_{growing}$), non-growing season temperature ($T_{non\text{-}growing}$), growing season precipitation ($P_{growing}$), and non-growing season precipitation ($P_{non\text{-}growing}$). Each composite is derived from normalized (0–1) constituent variables (Supplementary Fig. 3) following O'Donnell and Ignizio[12]. Boxes represent interquartile ranges (25th–75th percentiles); horizontal lines denote medians, and whiskers extend to 1.5 times the interquartile range. The vertical dotted line at 11.5 cal. ka BP marks the onset of the Holocene. All hemispheric-scale values were derived by averaging biome-grouped time series using area-weighted means, with weights based on the relative extent of each biome (Supplementary Table 4).

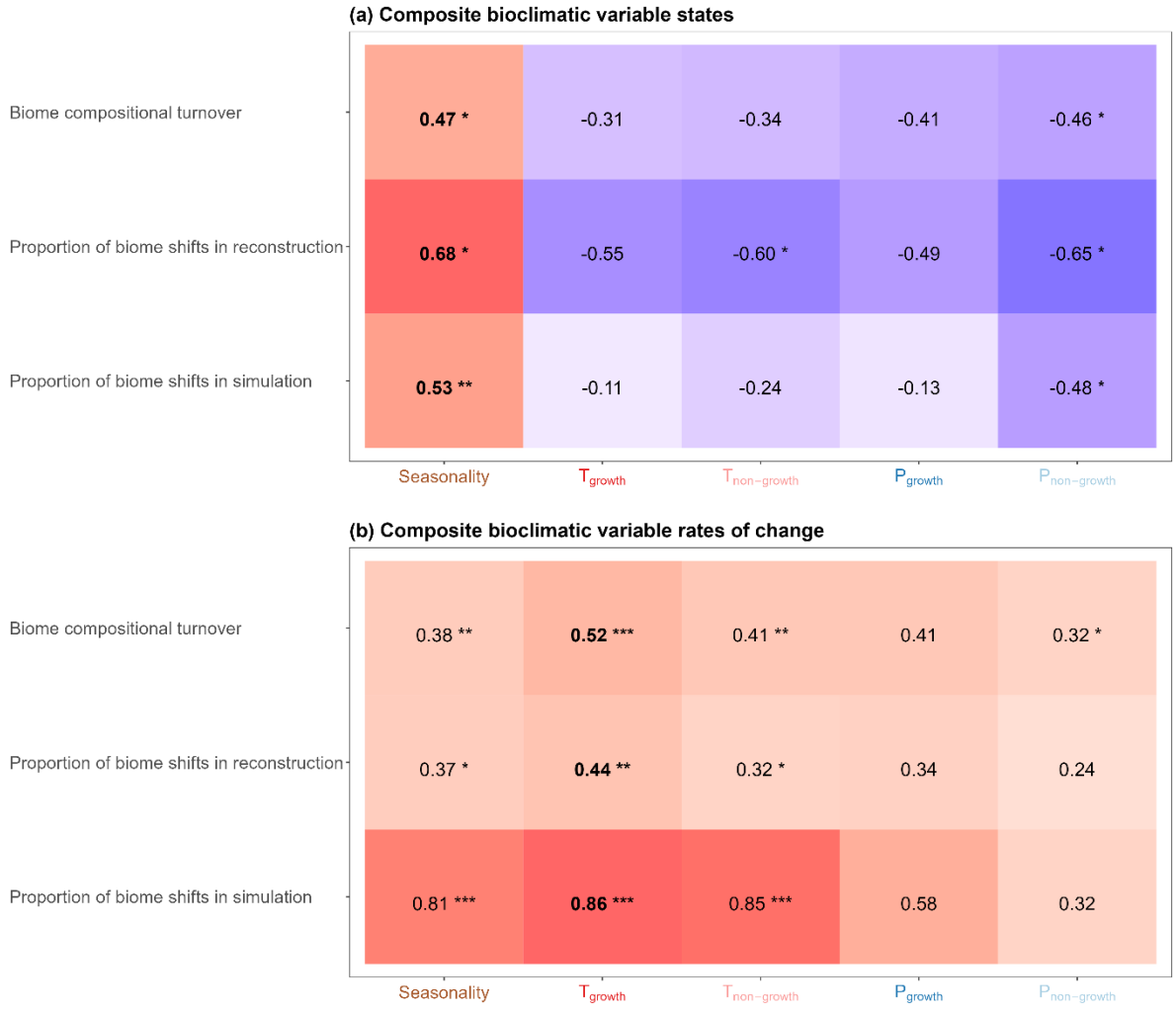
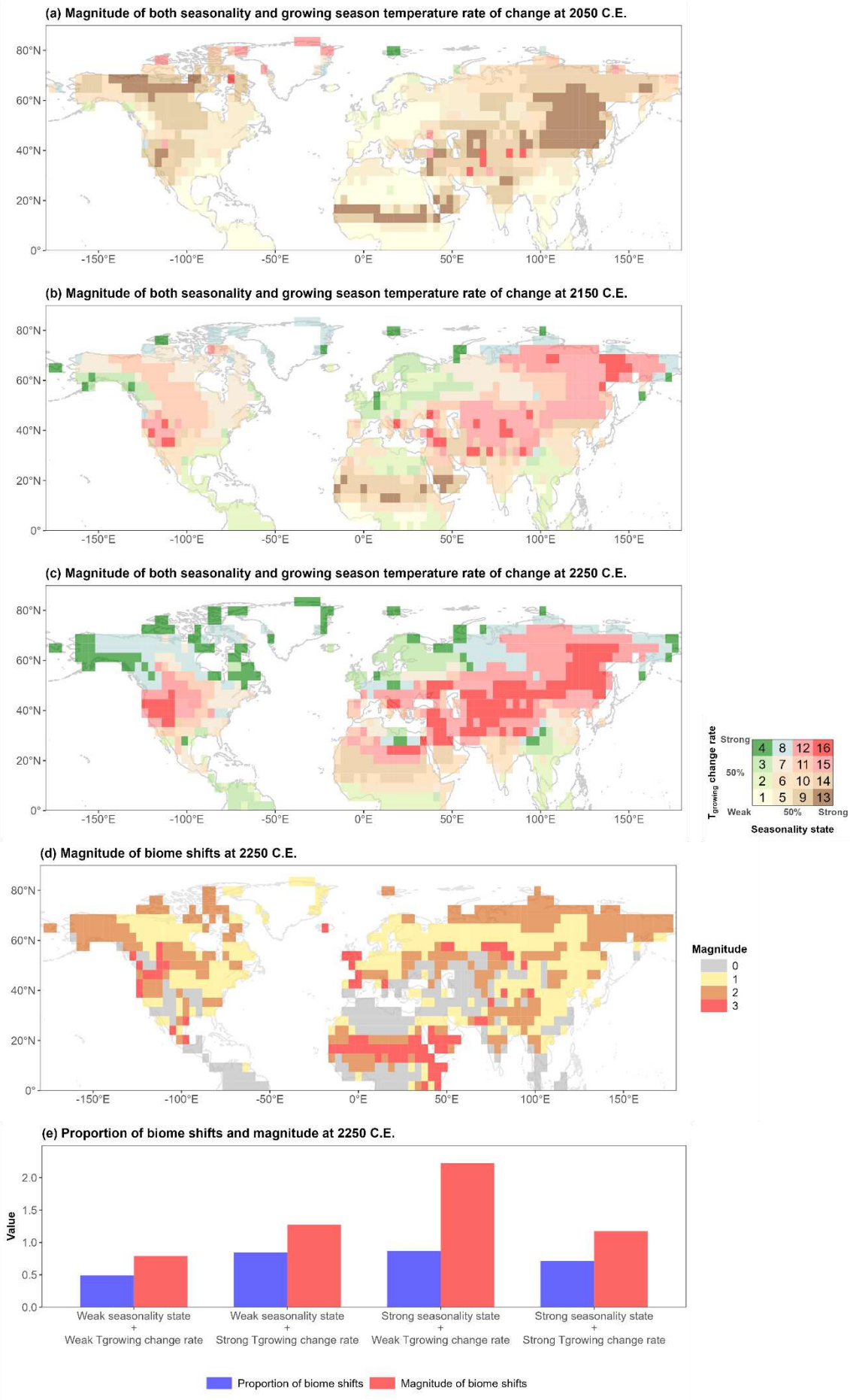


Fig. 3: Correlations between biome changes and (a) the state and (b) the rate of change of composite bioclimatic variables simulated by MPI-ESM[8,19] over the past 21,000 years in the Northern Hemisphere. Gaussian kernel correlation coefficients are shown between biome change metrics and simulated composite bioclimatic variables, including bioclimate seasonality (seasonality), growing season temperature ($T_{growing}$), non-growing season temperature ($T_{non\text{-}growing}$), growing season precipitation ($P_{growing}$), and non-growing season precipitation ($P_{non\text{-}growing}$). Each R-value represents the mean correlation across its constituent variables (see Supplementary Fig. 3); the highest value in each row is shown in bold. Asterisks denote significance based on the maximum *p*-value of the constituent variables[12]: * $p < 0.05$; ** $p < 0.01$; *** $p < 0.001$.


(a) Magnitude of both seasonality and growing season temperature rate of change at 2050 C.E.
(b) Magnitude of both seasonality and growing season temperature rate of change at 2150 C.E.
(c) Magnitude of both seasonality and growing season temperature rate of change at 2250 C.E.
80°N
60°N
40°N
20°N
0°
-150°E
-100°E
-50°E
0°E
50°E
100°E
150°E
Tgrowing change rate
Strong
50%
Weak
4 8 12 16
3 7 11 15
2 6 10 14
1 5 9 13
Seasonality state
(d) Magnitude of biome shifts at 2250 C.E.
Magnitude
0
1
2
3
(e) Proportion of biome shifts and magnitude at 2250 C.E.
Value
2.0
1.5
1.0
0.5
0.0
Weak seasonality state + Weak Tgrowing change rate
Weak seasonality state + Strong Tgrowing change rate
Strong seasonality state + Weak Tgrowing change rate
Strong seasonality state + Strong Tgrowing change rate
Proportion of biome shifts
Magnitude of biome shifts

40

Fig. 4: Future bioclimatic stress and projected biome shifts in the Northern Hemisphere based on the MPI-ESM simulation under a high-emission scenario (RCP 8.5[21]). (a–c) Spatial distribution of combined bioclimatic stress—defined by the magnitude of both bioclimate seasonality and the rate of change in growing season temperature ($T_{growing}$)—relative to pre-industrial conditions (timeslice: 0.1 cal. ka BP), shown for three future timeslices: 2050, 2150, and 2250 C.E. (Supplementary Data 3). Classifications (n = 16) are based on quantile combinations of each variable, with red indicating strongest seasonality and warming, and green indicating the weakest (see legend). **(d)** Projected magnitude of biome shifts at 2250 C.E., represented as an ordinal metric from 0 (no shift) to 4 (maximum shift), reflecting increasing dissimilarity in vegetation structure and bioclimatic affinity relative to pre-industrial baselines. **(e)** Proportion and magnitude of biome shifts at 2250 C.E., stratified by binary categories of seasonality and $T_{growing}$ change rate (weak/strong, based on 50% quantiles). Blue bars show the proportion of grid cells within each climatic stress class undergoing biome shifts; red bars represent the average shift magnitude across each class (Supplementary Table 2). All results are based on MPI-ESM transient simulations under the RCP 8.5 forcing scenario, at a spatial resolution of ~3.75° × 3.75°.

Supplementary Files

This is a list of supplementary files associated with this preprint. Click to download.

- Supplementaryinformation.pdf
- Supplementarydata.zip